Unified Model of Necking and Shear Banding in Amorphous and Semicrystalline Polymers

J. Sweeney, P. Caton-Rose, R. Spares, P. D. Coates

School of Engineering, Design, and Technology/IRC in Polymer Science and Technology, University of Bradford, Bradford BD7 1DP, United Kingdom

Received 17 November 2006; accepted 12 March 2007
DOI 10.1002/app.26546
Published online 8 July 2007 in Wiley InterScience (www.interscience.wiley.com).

ABSTRACT: In tensile stretching, many polymers undergo strain localization. The geometrical form of the localization can take the form of either a shear band or an approximately symmetric neck. We present a constitutive model of the early stages of deformation that predicts which form the localization will take. The model consists of an Eyring process acting with a Gaussian network that is implemented numerically. A Levy–Mises flow rule associated with the Eyring process has a tendency to produce shear bands. A relatively stiff Gaussian network is used in a model of polycarbonate that ensures that most of the strain is taken up by the Eyring process, resulting in shear banding. In contrast, a relatively soft Gaussian network is used in a model of polyethylene, which takes up the greater part of the strain, resulting in a neck. The predictions are compared with experiments. For polyethylene, a two-Eyring-process model is introduced for better accuracy. © 2007 Wiley Periodicals, Inc. J Appl Polym Sci 106: 1095–1105, 2007

Key words: necking; polycarbonates; polyethylene (PE)

INTRODUCTION

In some forms of polymer processing, such as thermoforming, film blowing, and die drawing, large strains are applied in the solid phase. For the accurate numerical modeling of these processes, the mechanical behavior of the polymer must be understood in terms of its constitutive equation, which has to encompass nonlinearity and strain-rate dependence. Ideally, the constitutive equation should function under all conditions, including those obtained at instabilities: high strain rates and extreme strain localization. This regime presents a rigorous challenge to the constitutive model, and this consideration has led us to study the problem of instability over a range of polymer materials.

In tensile stretching, many polymers extend nonuniformly after an initial stage of homogeneous deformation. The onset of nonuniformity is associated with a load drop. The dynamics of the process are well understood in terms of the underlying constitutive behavior of the material, which must be such that the uniaxial nominal stress–strain curve reaches a maximum in stress. Then, in a tensile specimen, a large strain can coexist with a small strain, and furthermore, this inhomogeneous state may be associated with lower strain energy than the corresponding uniform state, resulting in a neck or other form of strain localization. However, strain localization is accompanied by a local increase in the strain rate. In materials for which the stress depends on the rate of strain, an increase in stress would accompany the local increase in the strain rate, increase the strain energy associated with the nonuniform state, and thus favor homogeneous deformation. Sweeney et al.[1] described in detail how these competing effects affect the necking process in polymers.

Aside from the criterion that governs the existence or otherwise of an instability, there is the question of what geometric form it will take. In the uniaxial stretching of plane tensile specimens, there are two possibilities: a neck, symmetric about the specimen axis, and a shear band, an area of localization at an oblique angle to the axis. In this article, we present finite element models of both kinds of instability that are based on the same form of a constitutive equation. The models are compared with experimental results for shear-banding polycarbonate and necking polyethylene, and we show that the same underlying constitutive equation gives a unified representation of both forms of instability.

Previous work on shear bands

Shear bands have been recognized for many years as the preferred deformation mode for yielding ductile metals when the geometrical conditions are favorable. Figure 1 shows the general arrangement of a shear band occurring under the conditions of uniaxial tension. The lateral displacement of the specimen

Correspondence to: J. Sweeney (j.sweeney@bradford.ac.uk).

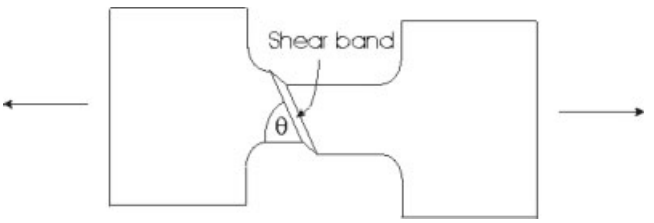

Figure 1 Tensile specimen with a shear band in the observed location.

ends is an essential component of this deformation, and the band itself consists of thinned material. Thus, in the terminology of Bowden,[2] our deformation is a combination of an inclined neck (the thinned region) and shear band (in which there is lateral displacement between the specimen ends but no thinning, with shear deformation only occurring along the band); we continue to refer to our combined deformation loosely as a shear band. The angle of inclination of the band to the tensile axis under these plane stress conditions has been calculated as $\tan^{-1}(\sqrt{2})$, that is, 54.74° for an incompressible material, on the basis that the band lies along the direction of zero elongational strain by Nadai.[3] Thomas[4] criticized this analysis for a lack of rigor and produced exact solutions based on both the von Mises and Tresca yield criteria. For both criteria, the same result of $\tan^{-1}(\sqrt{2})$ was returned, although in the case of Tresca, there was an additional result of $\tan^{-1}(\sqrt{2}/\sqrt{3})$. We are now satisfied that this latter result is nonphysical, as it corresponds to a tensile stress insufficient to cause yielding. Thomas[5] also predicted inclination angles for compressible materials, giving results as a function of Poisson's ratio and using an analysis that included the condition of zero elongational strain. This analysis also apparently produced more than one band angle for each condition, but we are satisfied that only one of them corresponds to both a sufficiently high stress and to the assumed plane stress conditions.

Shear bands in polymers have been reported for many years. Bauwens[6] measured the angles of bands in tensile specimens of rigid poly(vinyl chloride) and found them to be consistent with the prediction of 55° of Nadai[3] and Thomas.[4] Observations of the phenomenon specifically in polycarbonate also have a long history (e.g., Higuchi and Hyakutake[7] and Wu and Turner[8]). The tensile stress associated with the initiation of a macroscopic band is reproducible. Stress concentrations cause microshear bands to occur locally at a lower overall stress than that associated with the macroscopic band.[2,7]

More recently, the finite element method has been applied to investigate in detail the relationship between the material constitutive equation and the band geometry. Of particular relevance is the work of Lu and Ravi-Chandar,[9] who modeled the stretching of polycarbonate in uniaxial tension using a trilinear constitutive equation, which included no strain rate dependence of stress but captured some essential elements of the phenomenon. The assumption of incompressibility was made for the postyield behavior, and the modeled shear-band angles corresponded to the Nadai/Thomas 55° prediction. Simple tensile boundary conditions were used, and the localization of stress required for the initiation of the shear band was created by a local material inhomogeneity. Wu and van der Giessen[10,11] used more physically realistic constitutive equations to make finite element models of shear bands in polycarbonate and polystyrene. They constructed their constitutive model by combining Argon's mechanism of plastic flow[12] with an elastic response based on their full network polymer chain model,[13] an approach similar in spirit to that of Arruda and Boyce,[14] who used the eight-chain network[15] in place of the full network. The constitutive model of Wu and van der Giessen was implemented in finite element analyses and applied to shear bands occurring under conditions of applied compressive and shear strains.

Previous work on necks

Shear banding can be suppressed in glassy polymers by the selection of particular forms of specimen geometry, such as axisymmetry,[16–18] so that the inhomogeneity in strain is in the form of a symmetric neck. However, in some polymers, symmetric necking is invariably the observed form of inhomogeneity, independent of the specimen geometry. Thus, Brooks et al.,[19] Gaucher-Miri et al.,[20] Sweeney et al.,[21] and Unwin et al.[22] observed symmetric necks in plane tensile specimens of polyethylene. Polypropylene exhibits similar macroscopic behavior, as reported, for example, by Drozdov and Christiansen[23] and Sweeney et al.[24] The main distinguishing feature between polymers that neck and those that band appears to be that necking polymers undergo larger strains before the start of the instability. Recent work on multilayered poly(ethylene terephthalate)/polycarbonate tapes by Ivan'kova et al.[25] has suggested that an increased network density can transform the deformation mechanism into a shear band.

Necks in tensile specimens can be modeled successfully with the finite element method together with an appropriate constitutive equation. This has been done both for polypropylene[21,24] and for polyethylene.[26] In all these cases, the constitutive equations have been based on an elastic network model, with no flow rule and therefore no potential for shear banding. Although this approach reflects the observed behavior, there seems to be no fundamen-

tal physical reason for the inclusion of a flow rule for one class of polymer and its exclusion for another. In this article, we adopt a unified approach.

Constitutive model

Because we are concerned with the modeling of only the growth of the instability and are not considering subsequent events in the stretching of the specimen, a simple model is sufficient. For the majority of the models considered here, a single Eyring process acts in series with a Gaussian network, with the network and Eyring process associated with an elastic deformation gradient ($\mathbf{G^e}$) and a plastic deformation gradient ($\mathbf{G^p}$), respectively. For the total deformation gradient ($\mathbf{G}$)

$$\mathbf{G} = \mathbf{G^e}\mathbf{G^p} \tag{1}$$

An incremental time-stepping approach is adopted. Given $\mathbf{G}$, we use polar decomposition to obtain the total stretch ($\mathbf{D}$) and rigid body rotation ($\mathbf{R}$):

$$\mathbf{G} = \mathbf{D}\mathbf{R}$$

Suppose at some point in the analysis that the plastic stretch at the end of the previous time step is $\mathbf{D_0^p}$, $\Delta\mathbf{D^p}$ is the increment in the plastic stretch during the current time step, and $\mathbf{D^e}$ is the elastic stretch. Then, $\mathbf{G}$ is

$$\mathbf{G} = \mathbf{D^e}\Delta\mathbf{D^p}\mathbf{D_0^p}\mathbf{R} \tag{2}$$

where $\mathbf{D^e}$, $\Delta\mathbf{D^p}$, and $\mathbf{D_0^p}$ are symmetric tensors with no associated rigid body rotations. $\mathbf{D^e}$ and $\Delta\mathbf{D^p}$ are collinear and share principal directions that are in general different from those of $\mathbf{D_0^p}$. We follow Bonet and Wood[27] and make the initial estimate of $\mathbf{D^e}$, $\mathbf{D_i^e}$, by assuming that there is no additional plastic strain:

$$\mathbf{D_i^e} = \mathbf{G}\mathbf{R}^{-1}\mathbf{D_0^{p-1}}$$

For a given value of $\mathbf{G}$, $\mathbf{D^e}$ and $\Delta\mathbf{D^p}$ in eq. (2) are derived via an iterative process to impose the condition that the stresses in the network and the Eyring process are equal. Plane stress conditions are assumed. The Gaussian network is assumed to be incompressible, and the stress (σ_i) is given by the constitutive equation:

$$\sigma_i = C[\lambda_i^2 - (\lambda_\mathrm{I}\lambda_\mathrm{II})^{-2}] \tag{3}$$

where i is I or II; I and II are the principal directions in the plane; and λ_i is the principal extension ratio, which is equal to the diagonal entries of $\mathbf{D^e}$ when transformed along the principal directions. C defines the stiffness of the network.

We define the total stress tensor ($\boldsymbol{\sigma}$) and the stress deviator ($\boldsymbol{\tau}$) as follows:

$$\boldsymbol{\tau} = \boldsymbol{\sigma} - \bar{\sigma}I$$

where $\bar{\sigma}$ is the mean stress [$\bar{\sigma} = \frac{1}{3}\mathrm{tr}(\boldsymbol{\sigma})$]. We further define the octahedral shear stress (τ) as

$$\tau = \sqrt{\frac{1}{3}\boldsymbol{\tau}\cdot\boldsymbol{\tau}}.$$

According to the Eyring theory, the scalar plastic strain rate ($\dot{e}_p$) is related to σ and τ by

$$\dot{e}_p = A\exp(V_p\bar{\sigma})\sinh(V_s\tau) \tag{4}$$

where A, V_p, and V_s are material constants, the latter two being proportional to the pressure and shear activation volumes, respectively.[28,29] $\dot{e}_p$ is defined in terms of the plastic velocity gradient ($\mathbf{L^p}$):

$$\dot{e}_p = \sqrt{\frac{1}{3}\mathbf{L^p}\cdot\mathbf{L^p}}$$

$\mathbf{L^p}$ is itself defined in terms of the plastic deformation gradient as

$$\mathbf{L^p} = \mathbf{D^p}\mathbf{D^{p-1}}$$

To fully define $\mathbf{L^p}$, we acknowledge that it is collinear with the stress and stress deviator and assume that the material obeys the Levy–Mises flow rule. Then, in principal directions, we have

$$\frac{1}{\dot{e}_p}\begin{pmatrix} \dot{\lambda}_\mathrm{I}^p/\lambda_\mathrm{I}^p & 0 & 0 \\ 0 & \dot{\lambda}_\mathrm{II}^p/\lambda_\mathrm{II}^p & 0 \\ 0 & 0 & \dot{\lambda}_\mathrm{III}^p/\lambda_\mathrm{III}^p \end{pmatrix} = \frac{1}{\tau}\begin{pmatrix} \tau_\mathrm{I} & 0 & 0 \\ 0 & \tau_\mathrm{II} & 0 \\ 0 & 0 & \tau_\mathrm{III} \end{pmatrix} \tag{5}$$

where λ_I^p, λ_II^p, and λ_III^p are the principal plastic extension ratios and τ_I, τ_II, and τ_III are the principal stress deviators. The plastic strain increment ($\Delta\mathbf{D^p}$) in eq. (2) is determined under the assumption that the rate of strain is constant within the time step.

Although most of the material modeling here makes use of the constitutive theory outlined in eqs. (1)–(5), for a more accurate representation of polyethylene, a combination consisting of two such models acting in parallel is used. Distinguishing the separate arms of this model by subscripts $\mathbf{X}$ and $\mathbf{Y}$, the separation of elastic and plastic deformations requires two equations to replace eq. (1):

$$\mathbf{G} = \mathbf{G_X^e}\mathbf{G_X^p} = \mathbf{G_Y^e}\mathbf{G_Y^p} \tag{6}$$

Similarly, deformations and rotations are related as in eq. (2):

$$\mathbf{G} = \mathbf{D}_X^e \Delta \mathbf{D}_X^p \mathbf{D}_{0X}^p \mathbf{R} = \mathbf{D}_Y^e \Delta \mathbf{D}_Y^p \mathbf{D}_{0Y}^p \mathbf{R} \tag{7}$$

There is one Gaussian network in each arm of the model, characterized by stiffnesses C_X and C_Y and giving principal stresses σ_{iX} and σ_{iY} in response to principal extension ratios λ_{iX} and λ_{iY}:

$$\begin{aligned} \sigma_{iX} &= C_X\left(\lambda_{iX}^2 - (\lambda_{\mathrm{IX}}\lambda_{\mathrm{IIX}})^{-2}\right) \quad iX = \mathrm{IX}, \mathrm{IIX} \\ \sigma_{iY} &= C_Y\left(\lambda_{iY}^2 - (\lambda_{\mathrm{IY}}\lambda_{\mathrm{IIY}})^{-2}\right) \quad iY = \mathrm{IY}, \mathrm{IIY} \end{aligned} \tag{8}$$

where it is implicit that the principal directions IX, IY, IIX, and IIY are in general different from one another. The principal stresses correspond to stress tensors in global directions ($\boldsymbol{\sigma}_\mathbf{X}$ and $\boldsymbol{\sigma}_\mathbf{Y}$) for each arm, with the total stress given by

$$\boldsymbol{\sigma} = \boldsymbol{\sigma}_\mathbf{X} + \boldsymbol{\sigma}_\mathbf{Y} \tag{9}$$

Two Eyring processes, one for each arm, are characterized by

$$\begin{aligned} \dot{e}_{pX} &= A_X \exp(V_{pX}\bar{\sigma}_X)\sinh(V_{sX}\tau_X) \\ \dot{e}_{\mathrm{pY}} &= A_Y \exp(V_{pY}\bar{\sigma}_Y)\sinh(V_{sY}\tau_Y) \end{aligned} \tag{10}$$

Scalar strain rates $\dot{e}_{pX}$ and $\dot{e}_{pY}$, mean stresses $\bar{\sigma}_X$ and $\bar{\sigma}_Y$, and octahedral shear stresses τ_X and τ_Y are defined analogously to $\dot{e}_p$, $\bar{\sigma}$, and τ. Two flow rules such as eq. (5) are used to specify the evolution of plastic strains in response to the octahedral shear stresses in each arm. The same numerical procedures are used to obtain equilibrium within the X and Y arms as in the single-arm model of eqs. (1)–(5). We refer to the theory of eqs. (1)–(5) as the single-process model and that of eqs. (6)–(10) as the two-process model. The latter is in effect a generalization, to large strains and two dimensions, of the work of Ward and Wilding.[30]

These models share kinship with the other polymer constitutive equations that combine entropic networks and viscous processes. In some cases,[28,14,31] the networks differ fundamentally from the Gaussian network used here, in that they include a finite chain extensibility limit. We have adopted the Gaussian model for simplicity and because, in the experimental work described here, the extensibility limit is not approached. For the viscous process, the Argon approach[12] is sometimes adopted[14,31] as an alternative to the Eyring approach used here and elsewhere.[28] The two theories of viscous flow are difficult to distinguish experimentally.

EXPERIMENTAL

We have compared the uniaxial tensile behaviors of polycarbonate and polyethylene. The former was Bayer Macrolon with a weight-average molecular weight (M_w) in the range of 35,000–37,000 and a glass-transition temperature of 148°C;[32] it was obtained in a commercial sheet form 3 mm thick. The polyethylene had $M_w \approx 206{,}000$ and was supplied in the form of granules. Sheets 1.4 mm thick were made through compression molding at 160°C and quenching into water at room temperature. For both materials, plane tensile specimens were cut from the sheets with the geometry specified in Figure 2. Standard tensile grips were used to hold the specimen ends. They were stretched with an Instron testing machine incorporating an environmental chamber, which was operated at 100°C for the polyethylene specimens and at 130°C for polycarbonate. We adopted as a standard a constant testing speed of 1.667 mm/s, although additional tests at half and double this speed were used to establish the rate dependence of the stress.

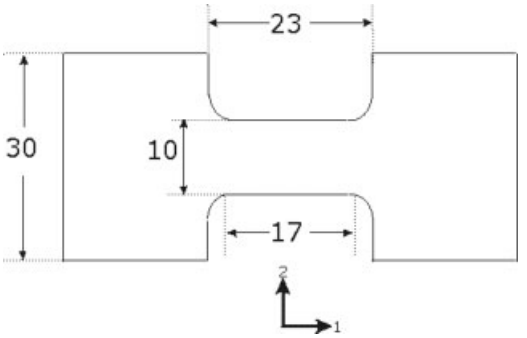

Figure 2 Specimen dimensions in millimeters. Stretching is along 1.

In the case of polycarbonate, in almost all cases, a shear band was initiated at one of the curved edges and became dominant [Fig. 3(a)]. In a minority of cases, a symmetric V-shaped pair of bands formed at one end. In a yet smaller number of cases, shear bands formed simultaneously at both ends. We conclude that there was usually some degree of deviation of the specimen and loading system from fourfold symmetry, which provided the condition necessary for the growth of a single shear band but was sometimes so small that the symmetric V-shaped pair of bands or bands at both ends were formed. Imperfection in the specimen and misalignment of its axis with respect to that of the testing machine are the obvious possible mechanical sources of asymmetry. There is also the likelihood that small temperature variations along the specimen would have a significant effect under these unstable conditions. The overall stress–deformation behavior of the specimens is highly reproducible and independent of the observed mode of deformation. In Figure 4, we show a typical nominal stress–time curve, which was formed from an average of 10 experiments under the standard conditions specified previously. The stress maximum corresponds to the onset of banding.

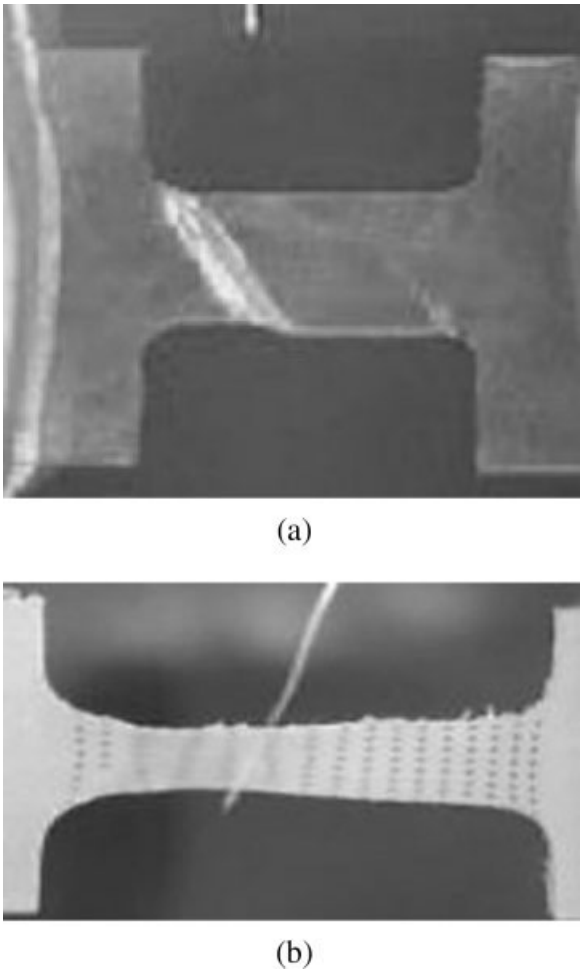

Figure 3 (a) Shear band in polycarbonate at 130°C and (b) neck in polyethylene at 100°C.

Optical microscopy of tested specimens has revealed microshear bands in the specimen gauge length, sometimes originating at the ends of cracks (Fig. 5). From printed images, measurements of the angles between associated microshear bands have enabled us to estimate the angle between the shear band and the tensile axis. Twenty-three such measurements of the material outside the shear band give a value of the angle to the tensile axis of 52.1 ± 2.4°, with the error corresponding to a 95% confidence interval. This is just significantly less than the 54.74° prediction for an incompressible material based on the direction of zero normal strain and still less than the value of 56.1° calculated on the same basis for a material with a Poisson's ratio of 0.45, a value recently supported by experimentation.[33] Because the microshear bands form at stress concentrations, it is clear that they form at low macroscopic strains, certainly much less than the strain corresponding to the peak stress, when the macroscopic shear band forms. Once formed, the microshear band will be subject to further straining, which will tend to decrease the angle that it makes with the loading axis. We have calculated that a permanent strain of 4% is sufficient to change the angle from an initial value of 56.1° to within the confidence interval associated with the observations; this level of permanent strain is within expectations.

The polyethylene specimens are drawn under tension into an approximately symmetric neck, as shown in Figure 3(b). Figure 6 shows the evolution of stress. Here we show a single typical curve; the reproducibility is such that peak nominal stresses differ by at most 4%. The stress begins by increasing

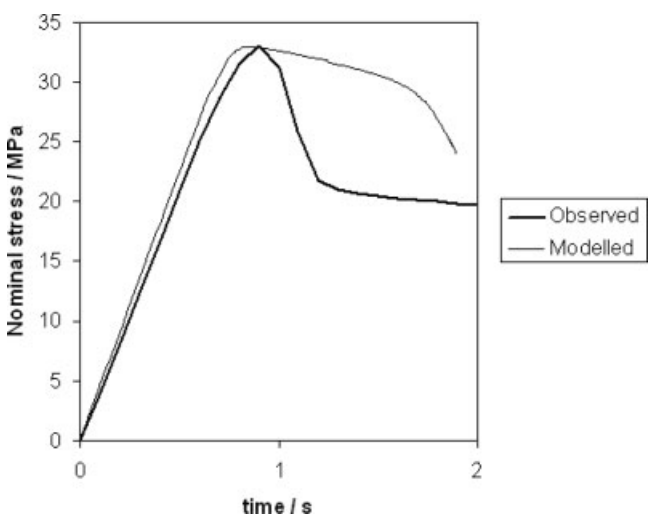

Figure 4 Observed and modeled results for the polycarbonate tensile tests.

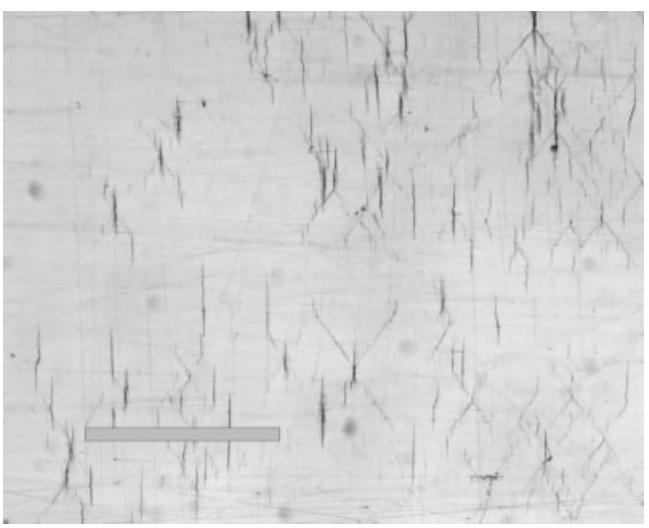

Figure 5 Optical micrograph of the specimen gauge length surface after stretching at 130°C along the horizontal direction. Microcracks and associated microshear bands are visible. The angles between shear bands originating at the same crack tip were used to estimate the angle of the shear band to the straining direction. The bar corresponds to a length of 500 μm.

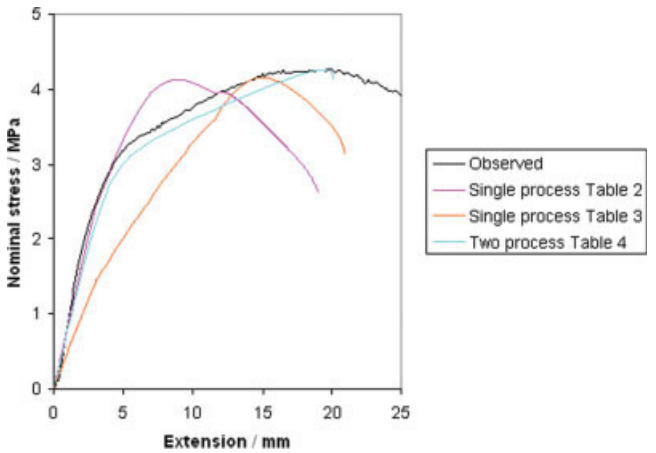

Figure 6 Observed and modeled results for polyethylene tensile tests. [Color figure can be viewed in the online issue, which is available at www.interscience.wiley.com.]

linearly, but around 3 s, the slope begins to decrease and thereafter follows further linear development at a shallower slope before reaching the stress maximum around 10 s. The slope change and stress maximum can be identified with separate Eyring processes, suggesting a model similar to that of Ward and Wilding[30] in their work on polyethylene fibers at room temperature.

Modeling

We have constructed a finite element model and applied it to experiments with both materials. Both materials are modeled with the constitutive relation defined in eqs. (1)–(5), with parameters defined appropriately for each material. Additionally, the polyethylene is modeled with the more sophisticated constitutive relation of eqs. (6)–(10). The mesh representing the tensile specimens, consisting of plane stress elements, is shown in Figure 7. The solutions were obtained with ABAQUS Standard, incorporating the constitutive equation as a UMAT user-defined subroutine.

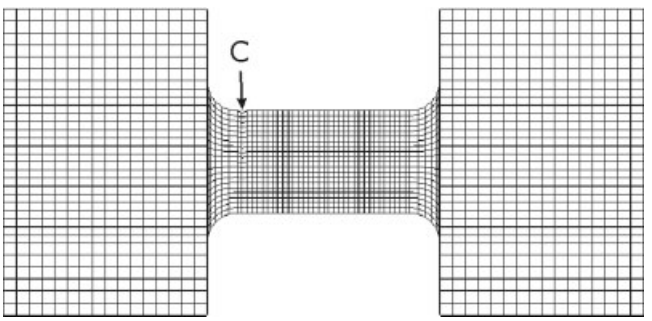

Figure 7 Finite element mesh for tensile specimens.

TABLE I
Model Parameters for Polycarbonate

C (MPa)	A (s^{-1})	V_s (MPa^{-1})	V_p (MPa^{-1})
385	2.0×10^{-18}	2.343	0.141

Polycarbonate

The greater challenge is posed by the shear-banding polycarbonate material. The mechanical properties are specified in Table I. The value of the Gaussian coefficient (C), 385 MPa, fits the observed initial slope of the stress–strain curve, but we note that it is of the same order as the 440 MPa value that we derive from the dynamic results of Govaert and Tervoort[34] for the testing temperature of 130°C. The observed rate dependence of the peak stress was used, via eq. (4), to fix the value of the combination $V_p + \sqrt{2}V_s$. This is possible under the assumption that the stress state is uniaxial, the hyperbolic sine function can be approximated by the exponential, and, at yield, the plastic strain rate is equal to the applied strain rate. This last feature is essential to a series model as proposed here.[35] To separate V_p and V_s, we have made use of estimations of the ratio V_p/V_s based on the work of other investigators. On the basis of the pressure dependence of the yield stress, Nazarenko et al.[18] proposed for polycarbonate $V_p/V_s = 0.06$, whereas Bauwens-Crowet and Bauwens[36] proposed 0.075, while noting values in the range of 0.05–0.072 obtained by other workers. During a comparison of ratios obtained by different authors, it becomes apparent that there are alternative values of V_s depending on the precise definition of the driving stress in eq. (4). Although here we use the octahedral shear stress $\sqrt{\boldsymbol{\tau}\cdot\boldsymbol{\tau}/3}$, other workers have used the effective stress $\sqrt{\boldsymbol{\tau}\cdot\boldsymbol{\tau}/2}$. Examples of the latter are Govaert et al.,[37] who used for polycarbonate a value of V_p/V_s that corresponds to 0.06 according to the definitions of this article. The ratio 0.06 is supported by experimental evidence and falls within the range of accepted values, and we have adopted it here. The separated values of V_p and V_s are given in Table I. The value of A is obtained through fitting to the observed maximum stress level in the tensile tests.

The aforementioned mechanical properties invariably result in shear-band predictions in tensile stretching. This is true both with the finite element mesh of Figure 7 (which is the basis of all the modeling results discussed here) and with less dense meshes having gauge lengths comprising a 30×12 rectangular array of elements, rather than this 34×20 array. However, the modeled position of the band will not in general be as observed experimentally, as it depends on the precise boundary conditions employed. In all cases, there is a condition of zero lateral strain applied to both boundaries, L and R

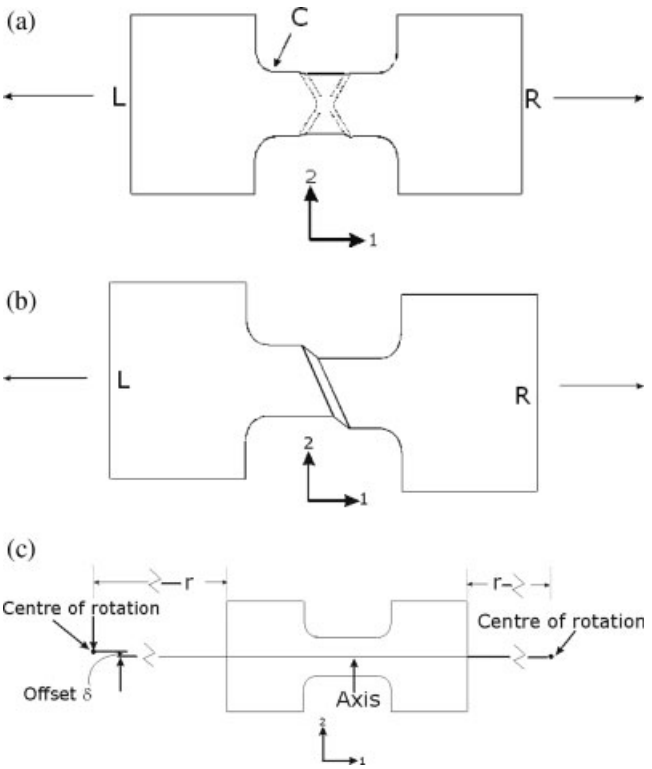

Figure 8 (a) Shear bands under symmetrical conditions, (b) a single shear band centrally located, and (c) boundaries rotating about offset centers.

(see Fig. 8), to simulate the action of tensile grips. Simple displacement boundary conditions, in which, in addition, boundaries *L* and *R* are both restrained laterally and axially separated, [see Fig. 8(a)] result in a symmetric solution with a pair of bands at the center of the specimen in an *X* formation. We know that the existence of a single band, as observed experimentally, requires that there be relative lateral movement between the specimen ends. There must be some initial asymmetry in the specimen or its setup to determine the sense of the larger asymmetry that develops as the band forms; this applies both to the model and to the real specimen. In practice, the most plausible source of asymmetry would be imperfections in the specimen (e.g., machining defects around the curved boundaries), off-axis loading, or temperature variations. We have explored combinations of the first two effects, bearing in mind that the typical experimental observation is that of a band growing from near one of the points *C* in Figure 8(a). The conditions are as follows:

1. We introduce a small flaw in the form of a 0.15-mm inward displacement of a node on the gauge length boundary near point *C* [see Fig. 8(a)]. There is no off-axis loading. We allow lateral (2 direction) movement of boundary *L*, while fixing it in the 1 direction and moving *R* along the 1 axis only. Then, a single band is formed, but at the center of the specimen [see Fig. 8(b)] rather than in the position observed. Further increasing the size of the flaw can result in the band originating from point *C* as observed experimentally, but an unrealistically large flaw (0.3 mm) is required.
2. A detailed consideration of the experimental loading system leads to the conclusion that the sideways motion of the specimen end is caused by rotation of the loading member about a pin joint, rather than displacement of the boundary purely along the 2 direction. In fact, both boundaries are potentially subject to this rotational condition. We have created conditions under which each boundary (*L* and *R*) is allowed to rotate about a point a fixed distance (*r*) from it, and the deformation is induced by the separation of the centers of rotations along the 1 axis. We have introduced asymmetry in the form of a realistic degree of offset loading by placing one of the centers of rotation a small distance (δ) from the specimen axis [see Fig. 8(c)]. With the rotation angles assumed to be small, linear equations linking the boundary nodal displacements are used to produce the required conditions, which are illustrated in Figure 8(c). The radii of rotation are determined by the geometry of the experimental loading system. With no flaw in the specimen, a single shear band is predicted at its center.
3. This is the same as condition 2, but with the addition of a flaw in the specimen at *C*. The shear-band positions are then as observed, provided that the flaw is 0.13 mm or larger. This is not a practically unrealistic flaw size, and as noted in the Experimental section, some asymmetry may be a result of temperature variation. We are not attempting to make a precise model of a real material flaw; the purpose of our model flaw is to provoke the observed pattern of strain localization. We accept that in reality some of the asymmetry may be of thermal rather than mechanical origin.

When using condition 3 with an offset loading of $\delta = 0.8$ mm, a radius of rotation of $r = 140$ mm, the properties in Table I, and an extension rate corresponding to the experimental value of 1.667 mm/s, we obtain the shear-banded shape shown in Figure 9. The angle of the shear band matches the theoretical value for incompressible materials discussed previously. The predicted nominal stress–time curve is compared with the experiment in Figure 4. The nominal stress is modeled well up to the peak value, but the drop in load is delayed by about 1 s in comparison with the experiment. The delay corresponds to the time required for the shear band to fully form after the peak load has

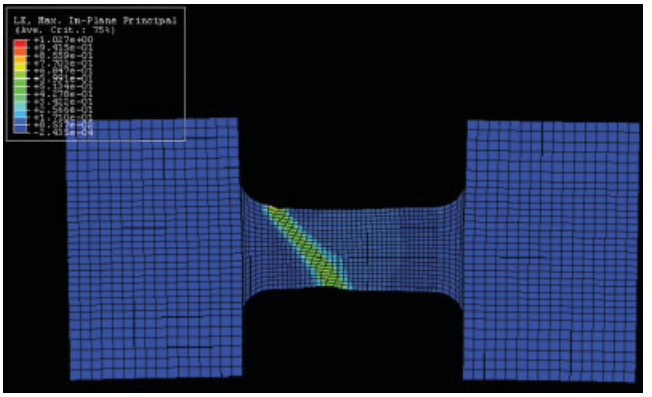

Figure 9 Finite element model of a tensile polycarbonate specimen with the material properties of Table I, showing the contours of the maximum principal true strain after 1.9 s. [Color figure can be viewed in the online issue, which is available at www.interscience.wiley.com.]

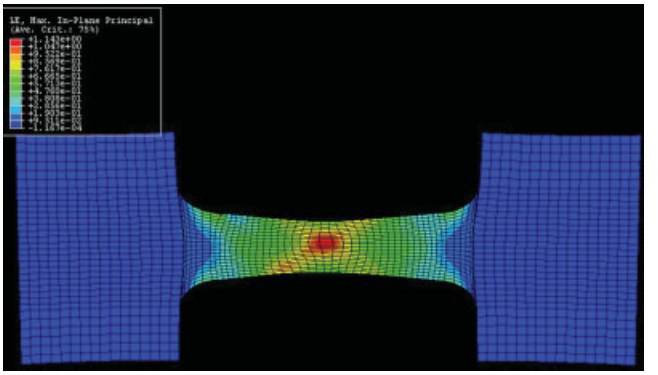

Figure 10 Finite element model of a tensile polyethylene specimen with the material properties of Table II, showing the contours of the maximum principal true strain after 11.4 s. [Color figure can be viewed in the online issue, which is available at www.interscience.wiley.com.]

been reached; in the experiments, the band forms in much less than 1 s. The parameters defining the Eyring process were obtained from the magnitude and rate dependence of the peak stress and so correspond to a uniform specimen strain and material at small strains. The material in the band is at strains of 40% or more and so may have different properties. The concept that the material will flow more freely after yield has been supported by the work of Zhou et al.[38] and Nanzai et al.,[39] who suggested that polycarbonate, on yielding, transforms temporarily from a glassy state into a rubbery state in which it flows more freely. Such complex behavior would not be captured by our simple model. As it stands, our model is a useful tool for exploring the development or otherwise of shear bands, although we accept that the speed of band development is not well modeled.

Because the degree of offset varies randomly between experiments while producing reproducible load–extension results, we require that the model results be insensitive to δ, provided that it lies within realistic limits. We have verified that using a value of $\delta = 1.6$ mm rather than 0.8 mm gives essentially indistinguishable predictions. We judge that the 0.8-mm offset is a reasonable expectation, given the visual alignment method used.

Polyethylene

Here the loading behavior, as illustrated in Figure 6, is more complex than that for polycarbonate, with two discernible slopes. The single-process model of eqs. (1)–(5) will predict only one slope value. However, we can make use of this model to approximate the behavior of polyethylene and show how the deformation behavior with respect to necking or shear banding is influenced.

For the polyethylene modeling, we have maintained the boundary and flaw conditions of condition 3. We have also retained the value $V_p/V_s = 0.06$. The values of V_s and A are selected pragmatically to fit the observed behavior and may not be unique in this respect. In Table II, we have chosen a value of C so that the initial slope of the stress–deformation curve is matched and chosen other parameter values to give the correct yield stress, which then occurs at too early a time. This is shown in Figure 6. The corresponding deformation field is shown in Figure 10, using the mesh of Figure 7 and the boundary conditions and flaw size as specified in condition 3. Given geometry and boundary conditions identical to those for the polycarbonate in Figure 9, it is clear that symmetric necking is now the dominant form of instability.

In Table III, the value of C is lower than in that Table II, so the yielding occurs at a realistic time, as shown in Figure 6. With geometry and boundary conditions identical to those for the previous case, the corresponding deformation field shown in Figure 11 again features necking as the form of instability. In this case, the neck is localized near the edge flaw.

For completeness, we introduce the more realistic two-process model with the material parameters

TABLE II
Model Parameters for Polyethylene: The Single-Process Model

C (MPa)	A (s^{-1})	V_s (MPa^{-1})	V_p (MPa^{-1})
11.9	5.6×10^{-5}	3.08	0.178

TABLE III
Model Parameters for Polyethylene: The Single-Process Model

C (MPa)	A (s^{-1})	V_s (MPa^{-1})	V_p (MPa^{-1})
7.0	5.6×10^{-5}	2.79	0.161

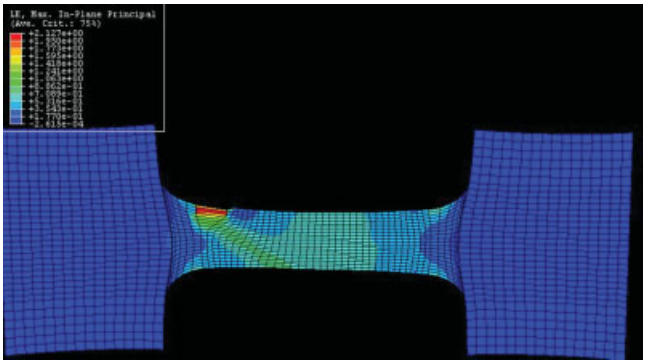

Figure 11 Finite element model of a tensile polyethylene specimen with the material properties of Table III, showing the contours of the maximum principal true strain after 12.6 s. [Color figure can be viewed in the online issue, which is available at www.interscience.wiley.com.]

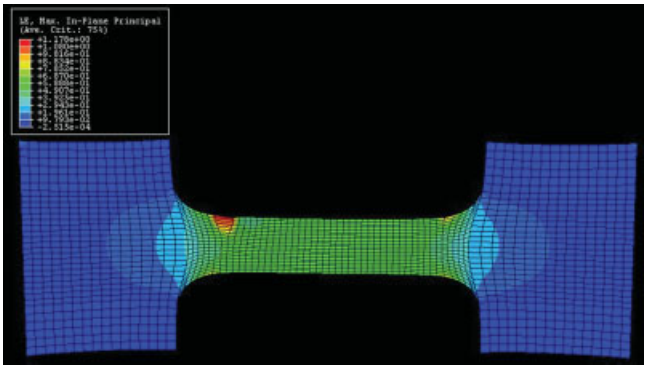

Figure 12 Two-process finite element model of a tensile polyethylene specimen with the material properties of Table IV, showing the contours of the maximum principal true strain after 12.1 s. [Color figure can be viewed in the online issue, which is available at www.interscience.wiley.com.]

specified in Table IV. Figure 6 shows that the stress–deformation curve is now modeled more accurately. The deformation field of Figure 12, obtained with the same geometry and boundary conditions as the two previous cases, exhibits the start of a neck, again close to the edge flaw.

We have included the edge flaw in the models of polyethylene to prove the point that, when we compare models based on polyethylene with those based on polycarbonate, the difference in the behavior is a result entirely of the constitutive equation because the geometries and boundary conditions are identical. However, we have also run the model with no flaw, using Table IV parameters, and found that the resulting strain fields are extremely similar; the loading offset is the primary cause of the location of the observed neck origin. The load–extension predictions are also virtually identical, and the results are independent of whether a large (0.8-mm) or small (1.6-mm) offset is used. A quantitative comparison with experimental strain fields is not possible because the strains associated with the initial stages of necking are not reproducible. In some cases, the neck develops symmetrically, but there are other cases in which it begins on one side of the specimen, resembling the prediction of Figure 12. It seems most likely that this is the result of various degrees of offset in the original specimen alignment. The load–extension curves and the shapes of the fully developed necks are, in contrast, satisfactorily reproducible.

As with polycarbonate, the rate of stress decay after the load peak is not well captured; in all cases in Figure 6, the predicted rates of decrease are greater than those observed. The Eyring parameters have been derived from the peak loads, at which the material is still at relatively small strain compared with the strain in the neck. Strains here are much higher than those in polycarbonate, and so the molecular orientation effects in the neck may become significant. In particular, Ward and Wilding[30] showed that the activation volume in polyethylene decreases with increasing orientation, and this would have the effect of decreasing the V_s parameter and lowering the rate of stress decay. This effect would not be captured in our model, in which the parameters are constant.

Transitional behavior

On comparing the mechanical properties of the two materials as specified in Table I for polycarbonate and in Tables II–IV for polyethylene, we find that there is a major difference between the stiffnesses of the Gaussian components, as defined by the parameter C. We believe that the relative stiffness of the Gaussian and Eyring mechanisms is the factor that governs whether the instability is in the form of a neck or a shear band. It is therefore of interest to attempt to observe the transition from one form of instability to the other as the stiffness ratio is varied. We have done this by taking the properties as defined in Table I and varying C while keeping the other parameters constant. As shown in Figure 13(a), shear-banding behavior persists as C is lowered to a value of 170 MPa, although there is some trace of the beginnings of a neck around where the band ini-

TABLE IV
Model Parameters for Polyethylene: The Two-Process Model

C_X (MPa)	C_Y (MPa)	A_X (s^{-1})	A_Y (s^{-1})	V_{sX} (MPa^{-1})	V_{pX} (MPa^{-1})	V_{sY} (MPa^{-1})	V_{pY} (MPa^{-1})
9.0	2.13	5.6×10^{-5}	7.03×10^{-15}	6.24	0.36	12.1	0.70

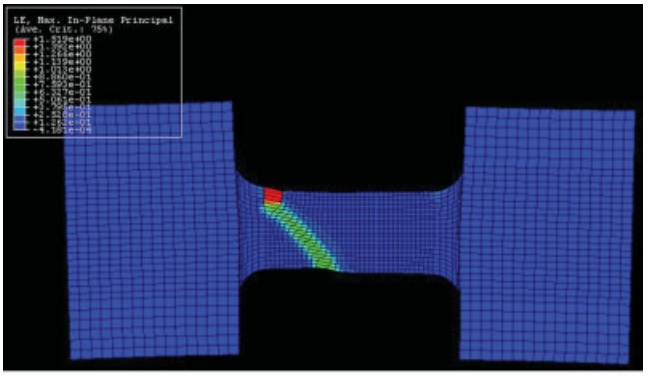

(a)

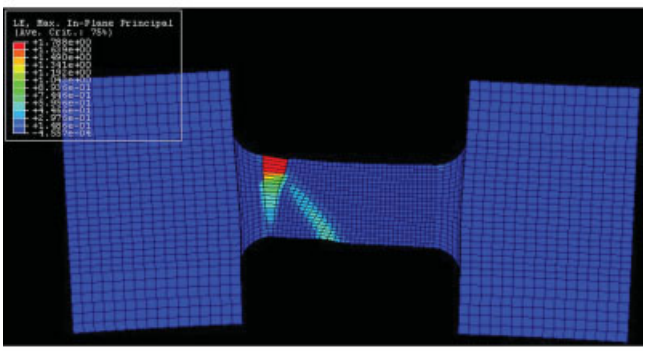

(b)

Figure 13 Contours of the maximum principal true strain after 2.5 s. The material parameters are the same as those in Table I, except that (a) C is 170 MPa (some of the band has been replaced by necked material) and (b) C is 165 MPa (the band has almost entirely been replaced by necked material). [Color figure can be viewed in the online issue, which is available at www.interscience.wiley.com.]

tiates. The result obtained with a further decrease in the value of C to 165 MPa is shown in Figure 13(b), in which necking behavior now clearly dominates. In this figure, the simulation has been allowed to progress to a stage at which, in reality, the material would be strain-hardening; because there is no strain hardening incorporated into this model, which is appropriate only for the initial stages of deformation, strains are higher and the degree of off-axis displacement is greater than would be realistic. However, we have successfully modeled the transition from banding to necking.

DISCUSSION AND CONCLUSIONS

A single constitutive equation, consisting of an Eyring process and a Gaussian network, can be used to model successfully the formation of instabilities in tensile specimens of both polycarbonate and polyethylene. This is significant as the geometrical form of instability is radically different for the two materials, being in the form of a shear band in polycarbonate and a symmetric neck in polyethylene. In both cases, finite element models give good predictions of both boundary forces and strain fields. The values used for the mechanical parameters specifying the model are comparable with those used by other workers in similar contexts.

In the case of polycarbonate, the boundary conditions applied to the model specimen have to be selected with particular care for the shear band to be predicted successfully. The single shear band that is observed experimentally requires some degree of asymmetry. This can be generated by a geometrical flaw in the material, but we found that the flaw size had to be unrealistically large if it was the sole source of asymmetry. The inevitable asymmetry under boundary conditions, which in practice results from offset loading, had to be incorporated into the model. The applied boundary conditions reflected the geometry of the experimental loading system, in which tensile grips rotate about pin joints. The same conditions were used for the polyethylene simulations.

The stiffness of the network with respect to that of the Eyring process determines whether a shear band or a neck is predicted. In the decomposition of the deformation into elastic and plastic components according to eq. (1), only the plastic part is governed by the flow rule of eq. (5). Because it is this flow rule that enables the existence of a shear band, it follows that a band (a feature of the total deformation) will be observed only when the plastic component is dominant. This will occur when the elastic mechanism is relatively stiff.

The behavior of polyethylene is more accurately portrayed with a two-process model with two Eyring processes and two Gaussian networks. The strain predictions of necking rather than shear banding are essentially unchanged in comparison with the simpler model.

The authors thank Alan Duckett of the IRC in Polymer Science and Technology, University of Leeds, United Kingdom, for useful and stimulating discussions.

References

1. Sweeney, J.; Shirataki, H.; Unwin, A. P.; Ward, I. M. J Appl Polym Sci 1999, 74, 3331.
2. Bowden, P. B. In The Physics of Glassy Polymers; Haward, R. N. Ed.; Applied Science: London, 1973.
3. Nadai, A. Theory of Flow and Fracture of Solids, 2nd ed.; McGraw-Hill: New York, 1950.
4. Thomas, T. Y. Proc Natl Acad Sci USA 1953, 39, 257.
5. Thomas, T. Y. Proc Natl Acad Sci USA 1953, 39, 266.
6. Bauwens, J.-C. J Polym Sci Part A-2: Polym Phys 1967, 5, 1145, 1967.
7. Higuchi, M.; Hyakutake, H. Rep Res Inst Appl Mech 1968, 16, 265.

8. Wu, W.; Turner A. P. L. J Polym Sci Polym Phys Ed 1973, 11, 2199.
9. Lu, J.; Ravi-Chandar, K. Int J Solids Struct 1999, 36, 391.
10. Wu, P. D.; van der Giessen, E. Int J Solids Struct 1994, 31, 1493.
11. Wu, P. D.; van der Giessen, E. Eur J Mech A/Solids 1996, 15, 799.
12. Argon, A. S. Philos Mag 1973, 28, 839.
13. Wu, P. D.; van der Giessen, E. Mech Res Commun 1992, 19, 427.
14. Arruda, E. M.; Boyce, M. C. Int J Plasticity 1993, 9, 697.
15. Arruda, E. M.; Boyce, M. C. J Mech Phys Solids 1993, 41, 389.
16. Boyce, M. C.; Arruda, E. M. Polym Eng Sci 1990, 30, 1288.
17. Boyce, M. C.; Montagut, E. L.; Argon, A. S. Polym Eng Sci 1992, 32, 1073.
18. Nazarenko, S.; Bensason, S.; Hiltner, A.; Baer, E. Polymer 1994, 35, 3883.
19. Brooks, N. W.; Duckett, R. A.; Ward, I. M. Polymer 1992, 33, 1872.
20. Gaucher-Miri, V.; François, F.; Séguéla, R. J Polym Sci Part B: Polym Phys 1996, 34, 1113.
21. Sweeney, J.; Collins, T. L. D.; Coates, P. D.; Ward, I. M. Polymer 1997, 38, 5991.
22. Unwin, A. P.; Duckett, R. A.; Ward, I. M.; Collins, T. L. D.; Sweeney, J.; Coates, P. D. J Appl Polym Sci 2002, 86, 3135.
23. Drozdov, A. D.; Christiansen, J. D. Polymer 2002, 43, 4745.
24. Sweeney, J.; Collins, T. L. D.; Coates, P. D.; Duckett, R. A. J Appl Polym Sci 1999. 72, 563.
25. Ivan'kova, E. M.; Michler, G. H.; Hiltner, A.; Baer, E. Macromol Mater Eng 2004, 289, 787.
26. Sweeney, J.; Collins, T. L. D.; Coates, P. D.; Duckett, R. A.; Ward, I. M. Int J Plasticity 2002, 18, 399.
27. Bonet, J.; Wood, R. W. Nonlinear Continuum Mechanics for Finite Element Analysis; Cambridge University Press: Cambridge, England, 1997.
28. Buckley, C. P.; Jones, D. C. Polymer 1995, 36, 3301.
29. Spathis, G.; Kontou, E. Polym Eng Sci 2001, 41, 1337.
30. Ward, I. M.; Wilding, M. A. J Polym Sci Polym Phys Ed 1984, 22, 561.
31. Wu, P. D.; van der Giessen, E. Int J Mech Sci 1993, 35, 935.
32. Lundberg, L.; Jansson, J.-F. Polymer 1994, 35, 2084.
33. Siviour, C. R.; Walley, S. M.; Proud, W. G.; Field, J. E. Polymer 2005, 46, 12456.
34. Govaert, L. E.; Tervoort, T. A. J Polym Sci Part B: Polym Phys 2004, 42, 2041.
35. Ward, I. M.; Sweeney, J. An Introduction to the Mechanical Properties of Solid Polymers, 2nd ed.; Wiley: Chichester, England, 2004.
36. Bauwens-Crowet, C.; Bauwens, J.-C. J Mater Sci 1972, 7, 176.
37. Govaert, L. E.; Timmermans, P. H. M.; Brekelmans, W. A. M. J Eng Mater Technol 2000, 122, 177.
38. Zhou, Z.; Chudnovsky, A.; Bosnyak, C. P.; Sehanobish, K. Polym Eng Sci 1995, 35, 304.
39. Nanzai, Y.; Yamasaki, T.; Yoshioka, S. JSME Int J Ser A Solid Mech Mater Eng 1998, 41, 31.